JOURNAL OF SOLID STATE CHEMISTRY 108, 29–36 (1994)

Perovskite-like Solid Solutions in the System $LiTaO_3$–$CaZrO_3$

R. I. Smith[1] and A. R. West

Department of Chemistry, University of Aberdeen, Meston Walk, Old Aberdeen, AB9 2UE, Scotland, United Kingdom

Received May 7, 1992; in revised form April 15, 1993; accepted April 15,1993

An investigation of the $LiTaO_3$–$CaZrO_3$ phase diagram has been carried out and the solid solution limits redetermined. $LiTaO_3$ solid solutions extend from 0 to 20 mole% $CaZrO_3$. $CaZrO_3$ solid solutions cover the range 27 to 100 mole% $CaZrO_3$, but are incomplete since a two-phase region or immiscibility gap occurs over the range ~88 to 95 mole% $CaZrO_3$. The crystal structures of two perovskite-like $CaZrO_3$ solid solutions, one on either side of the immiscibility gap, were determined by Rietveld refinement of powder neutron diffraction data. The structures of these perovskite-like materials are compared and possible causes of the solid solution immiscibility are discussed. © 1994 Academic Press, Inc.

INTRODUCTION

$LiNbO_3$ and $LiTaO_3$ are important ferroelectrics (1–3) and are interesting host materials for electrooptic, electroacoustic and nonlinear optical devices. Doping with hydrogen and some transition metals modifies certain physical properties, such as refractive index and Curie temperature, T_C, of the host and the resulting materials find applications as, e.g., wave-guides (4–7). Previous studies (7–9) on the doping of $LiNbO_3$ and $LiTaO_3$ with H, Zr, and $CaZrO_3$ reported the formation of new phases whose X-ray powder patterns all have a certain similarity.

Neurgaonkar *et al.* (9) reported an "unidentified new phase" in the $LiTaO_3$–$CaZrO_3$ system for compositions between 21 and 70 mole% $CaZrO_3$. Rice (7) reported monoclinic $Li_{1-x}H_xNbO_3$, $0.75 < x < 0.77$, as having the same structure as MnF_3 (10), and being only the second known example of this structure type. Villafuerte-Castrejón and West (8) initially suspected their solid solution phases *X* and *Y*, in the Li_2O–Ta_2O_5–ZrO_2 and Li_2O–Nb_2O_5–ZrO_2 ternary systems, actually to be two-phase mixtures containing new cubic perovskites and a second, impurity phase. Later, these patterns were shown to be single phases which could be indexed on an orthorhombic unit cell similar to that of the orthorhombic perovskites (11). The powder patterns of phases *X* and *Y* were seen also to be similar to those of Neurgaonkar's new phase and Rice's monoclinic $Li_{0.23}H_{0.77}NbO_3$.

Because of these similarities in the powder patterns, further investigations were carried out on the new phase in the $LiTaO_3$–$CaZrO_3$ system. The phase diagram of the $LiTaO_3$–$CaZrO_3$ join was reinvestigated, allowing the stoichiometry ranges and thermal stability of the various solid solution phases to be determined.

Due to the very high melting temperatures in this system, it was not found possible to prepare crystals of size suitable for a single crystal structure study. Consequently, structural studies were performed using powdered samples. Neutron diffraction was chosen since these materials contained lithium in the presence of tantalum, zirconium, and calcium.

EXPERIMENTAL

Starting materials were Li_2CO_3 (BDH, 99%), Ta_2O_5 (BDH, 99.9%), Nb_2O_5 (Aldrich, 99.9%), $CaCO_3$ (BDH, 99.5%), and ZrO_2 (Ventron, 99+%). Large batches of $LiTaO_3$ and $CaZrO_3$ were prepared by reacting together the appropriate reagents in Pt crucibles, initially both at 800°C for 2–3 hr to expel CO_2, before final firing at 1000°C for 18 hr and 1350°C for 7 hr respectively, to complete the reactions. Compositions on the $LiTaO_3$–$CaZrO_3$ join were then prepared by reacting together suitable quantities of $LiTaO_3$ and $CaZrO_3$, again in Pt crucibles. Pelleted samples were reacted at temperatures between 1000 and 1350°C for 2 to 3 days, depending upon composition. No covering powder was used during sample preparation. Reaction products were determined by powder X-ray diffraction using a Philips Guinier–Hägg camera, $CuK_{\alpha 1}$ radiation, $\lambda = 1.5405$ Å.

For determination of the $LiTaO_3$–$CaZrO_3$ phase diagram, quenching experiments were carried out. Small amounts of sample, contained in platinum foil envelopes, were annealed at temperatures in the range 1500 to 1550°C before being rapidly cooled by dropping into a dish of mercury at room temperature. The products were carefully removed from the envelopes and examined by powder X-ray diffraction, as above.

[1] Present address: The ISIS Facility, Rutherford Appleton Laboratory, Chilton, Didcot, Oxfordshire, OX11 0QX, U.K.

0022-4596/94 $6.00

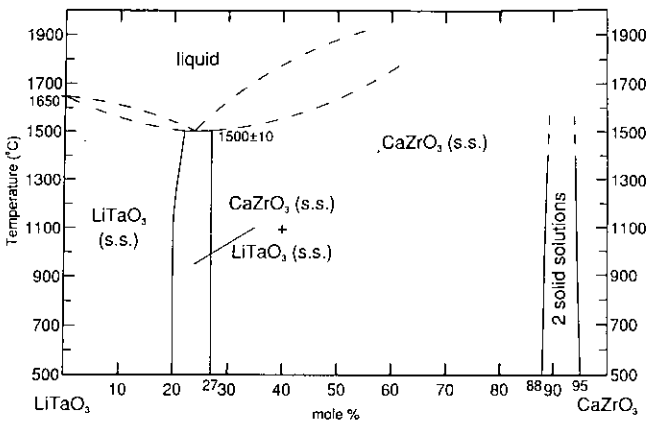

FIG. 1. The $LiTaO_3$–$CaZrO_3$ phase diagram.

Structural studies on two calcium zirconate solid solutions were carried out by Rietveld refinement (12) of time of flight powder neutron diffraction data. Data were collected on the Polaris medium resolution diffractometer at the U.K. spallation neutron source ISIS, Rutherford Appleton Laboratory, over the time of flight range 200–20,000 μsec with the 2900–18,000 μsec region (corresponding to a d-spacing range 0.47–2.92 Å at backscattering angles) used in structure refinement. The refinement program TF14LS, based on the Cambridge Crystallographic Subroutine Library (13), was used in which the experimental peak shape was modelled by a Voigt function convoluted with a double exponential decay. Neutron scattering lengths were taken from reference (14).

Samples for neutron diffraction data collection were prepared as above but using isotopically enriched $^7Li_2CO_3$ (A.E.R.E. Harwell, Stable Isotope Unit, 99.99% ^7Li).

RESULTS

$LiTaO_3$–$CaZrO_3$ Phase Diagram

The X-ray powder patterns of samples prepared on the $LiTaO_3$–$CaZrO_3$ joint showed the presence of three single phase regions, Fig. 1. At the two ends of the phase diagram, limited ranges of $LiTaO_3$ and $CaZrO_3$ solid solutions are formed, with solid solution limits at 20 and 95 mole% $CaZrO_3$ respectively. At intermediate compositions, 27 to 88 mole% $CaZrO_3$, an extensive range of perovskite-like solid solutions forms. The powder patterns of these latter solid solutions and the $CaZrO_3$ solid solutions both showed reflections characteristic of an orthorhombic perovskite. Solid solution limits were determined by careful examination of Guinier–Hägg films of reacted samples, showing the presence or absence of second phases.

The two perovskite powder patterns are very similar but with small differences in d spacings and hence unit cell dimensions, Figs. 2 and 3. Consequently, in the two phase region between 88 and 95 mole% $CaZrO_3$ the patterns were orthorhombic perovskite-like but with every line split into doublets and with relative intensities given by the volume fraction of the two components.

Phase diagram studies at high temperatures indicated a narrowing of this two phase region, and it is possible that at still higher temperatures it disappears to give a continuous perovskite solid solution range from 27 to 100 mole% $CaZrO_3$. In this case the two phase region between 88 and 95 mole% $CaZrO_3$ is part of a solid solution immiscibility dome.

In order to determine the upper limit of stability of the various solid solutions on the $LiTaO_3$–$CaZrO_3$ join, preliminary studies on the melting temperatures of powder samples were made. For most of the system the melting temperatures were above 1550°C, the maximum temperature of the furnaces used in these experiments; however, they are seen to pass through a minimum of 1500 ± 10°C at a eutectic separating the $LiTaO_3$ and Ca ZrO_3 solid solution regions, Fig. 1.

To further investigate the perovskite solid solution mechanism and the immiscibility dome, structure deter-

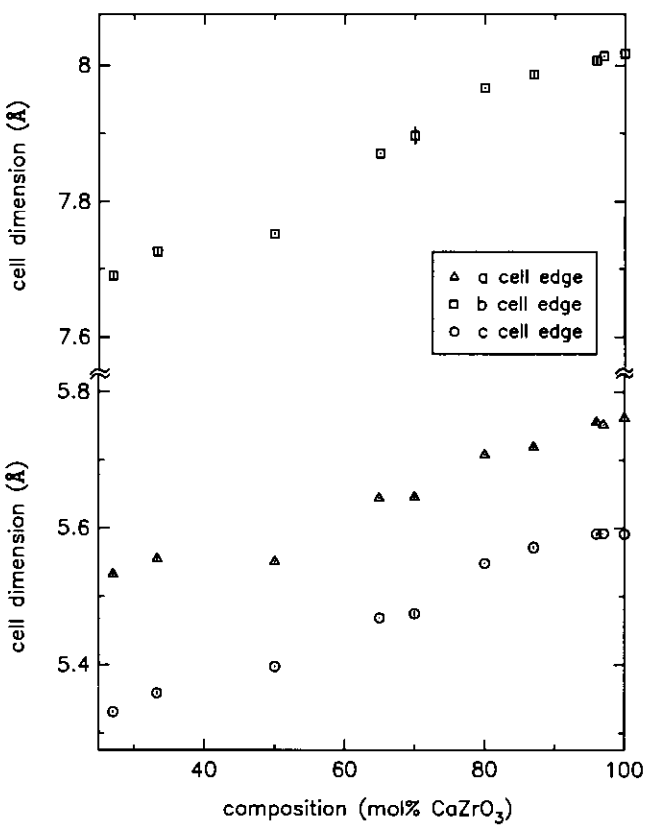

FIG. 2. Variation with composition of $CaZrO_3$ solid solution unit cell parameters. Parameters for $CaZrO_3$ taken from (15), parameters for 70 mole% $CaZrO_3$ composition calculated from Ref. (9) (see Table 5).

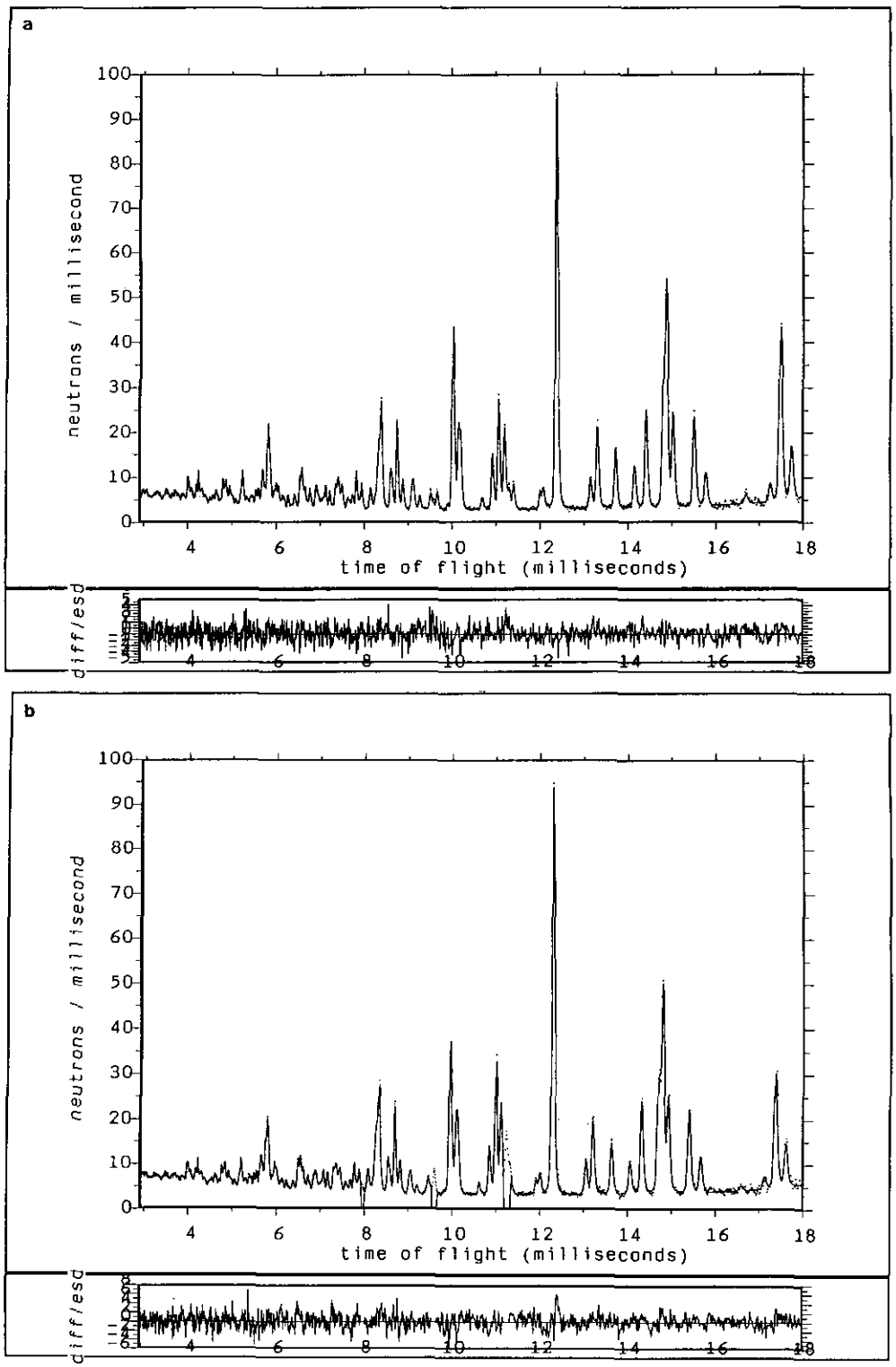

FIG. 3. Fitted powder neutron diffraction profiles for (a) $(CaZr)_{0.97}(LiTa)_{0.03}O_3$ and (b) $(CaZr)_{0.8}(LiTa)_{0.2}O_3$.

minations were carried out on two single phase $CaZrO_3$ solid solutions close to each of the solid solution immiscibility limits: compositions studied were $(CaZr)_{0.8}(LiTa)_{0.2}O_3$ and $(CaZr)_{0.97}(LiTa)_{0.03}O_3$.

Structural Studies Using Powder Neutron Diffraction Data

Time-of-flight powder neutron diffraction data from $(CaZr)_{0.8}(LiTa)_{0.2}O_3$ and $(CaZr)_{0.97}(LiTa)_{0.03}O_3$ solid solutions show very similar diffraction profiles, Fig. 3. Allowing for a difference in unit cell sizes, the distribution of positions and relative intensities of the reflections were very similar in both patterns. This provides further evidence, on top of the X-ray results, that these materials may be structurally related.

The structural model for Rietveld refinement used the atomic coordinates of orthorhombic $CaZrO_3$ (15). Zr and Ta were assumed to be disordered over the octahedral sites and Ca was located on the distorted 8-coordinate site. The occupancies of these sites were then refined in order to get an estimate of their total scattering before deciding on the actual site contents. Li atoms were not included in the initial refinements, the intention being to use difference Fourier maps in the later stages of structure refinement to locate these atoms.

Initially only scale, background, unit cell and peak shape parameters were varied. In subsequent refinements, positional, thermal, and site occupancy parameters were also refined.

$(CaZr)_{0.97}(LiTa)_{0.03}O_3$. Structure refinements of this solid solution composition were carried out in the orthorhombic space group *Pnma* (No. 62 (16)). The starting unit cell parameters were determined from an accurately measured Guinier–Hägg film. The occupancy of the *A* site, determined by the chemical formula, was initially fixed at $n = 0.97$.

The initial refinements of scale factor, background, unit cell, peak shape, and atomic positional parameters confirmed the perovskite-like starting model. However, results from subsequent refinements involving site occupancy and isotropic thermal parameters showed the calcium site to have an occupancy significantly less than the expected value of 0.97. Therefore, the possibility of lithium, which has a negative scattering length for neutrons, also occupying this site was investigated. The *A* site, however, would seem to be rather large for lithium occupation.

Allowing both Li and Ca to occupy the *A* site and refining the $CaZrO_3$ and $LiTaO_3$ contents of the cell indicated site contents of 0.96 Ca, 0.04 Li. These refined occupancies agreed well with the values of 0.97 and 0.03 expected from the chemical formula. The *A* site was therefore assumed to contain both calcium and lithium, with site occupancies fixed at $n = 0.97$ for calcium and $n = 0.03$ for lithium. The simultaneous refinement of calcium and lithium site occupancy and thermal parameters was made more reliable by the ability to collect short d-spacing data with the Polaris diffractometer (down to ~0.47 Å was used in structure refinement, Fig. 3). The assumed disorder of zirconium and tantalum on the *B* sites also appeared to be correct, with no evidence found for ordering.

TABLE 1
Cell and Atomic Parameters for $(CaZr)_{0.97}(LiTa)_{0.03}O_3$

Orthorhombic, *Pnma*, $Z = 4$
$a = 5.7515(1)$ Å, $b = 8.0138(2)$ Å, $c = 5.5922(1)$ Å

Atom	Pos.	x	y	z	B_{iso} (Å²)	n
Ca	4(*c*)	0.0483(2)	0.25	−0.0110(3)	0.55(2)	0.97
Li	4(*c*)	0.0483(2)	0.25	−0.0110(3)	0.55(2)	0.03
Zr	4(*b*)	0.0	0.0	0.5	0.25(1)	0.97
Ta	4(*b*)	0.0	0.0	0.5	0.25(1)	0.03
O(1)	4(*c*)	−0.0377(2)	0.25	0.3976(2)	—	1.00
O(2)	8(*d*)	0.2991(2)	0.0538(1)	0.6985(2)	—	1.00

Anisotropic temperature factors (Å²)

	B_{11}	B_{22}	B_{33}	B_{23}	B_{13}	B_{12}
O(1)	0.61(4)	0.15(3)	0.66(3)	—	0.02(3)	—
O(2)	0.46(2)	0.83(3)	0.49(2)	0.15(2)	−0.24(2)	−0.21(2)

Note. Esd's in parentheses.

In the final refinements anisotropic temperature factors were successfully refined for the oxygen atoms. Refinement terminated with $R_{wp} = 2.23\%$, $R_{ex} = 1.71\%$, $\chi^2 = 1.69$ for 1827 data points, and 38 variable parameters (for a definition of the *R* factors, see ref. (12)). Final refined unit cell and atomic parameters are given in Table 1, with selected bond distances and angles in Table 2.

$(CaZr)_{0.8}(LiTa)_{0.2}O_3$. This solid solution composition was found to have a structure very similar to that of $CaZrO_3$ and $(CaZr)_{0.97}(LiTa)_{0.03}O_3$, as was suspected from its X-ray powder pattern. Structure refinements were also carried out in the space group *Pnma* and the starting structural model was that of orthorhombic $CaZrO_3$. The *A* site occupancy, determined by the chemical formula, was fixed at $n = 0.80$.

Cell parameters determined from an accurately measured Guinier–Hägg film were used in the initial refinements of scale factor, background, and peak shape parameters. Subsequent refinements of unit cell parameters and oxygen and calcium positional parameters confirmed that this composition also had an orthorhombic perovskite-like structure. Oxygen, calcium and zirconium/tantalum atoms were in essentially the same positions as in $CaZrO_3$ and $(CaZr)_{0.97}(LiTa)_{0.03}O_3$. Further refinements of thermal and site occupation parameters confirmed that zirconium and tantalum were disordered over the *B* sites and that the *A* site was partially occupied, containing calcium only.

TABLE 2
Selected Bond Distances and Angles for $(CaZr)_{0.97}(LiTa)_{0.03}O_3$

Ca coordination		Li coordination	
Ca–O(1)	2.338(2)	Li–O(1)	2.338(2)
–O(1′)	2.464(2)	–O(1′)	2.464(2)
–O(2)	2.372(1) × 2	–O(2)	2.372(1) × 2
–O(2′)	2.681(2) × 2	O(1)–Li –O(1′)	87.30(6)
–O(2″)	2.841(1) × 2	–O(2)	107.72(5) × 2
		O(1′)–Li–O(2)	134.25(4) × 2
Zr/Ta coordination		O(2)–Li –O(2′)	83.01(6)
Zr/Ta–O(1)	2.095(1) × 2		
–O(2)	2.092(1) × 2	O coordination	
–O(2′)	2.089(1) × 2	Zr–O(1)–Zr′	146.0(1)
O(1)–Zr/Ta–O(1′)	180.0	Zr–O(2)–Zr′	147.2(1)
–O(2)	91.89(4) × 2		
–O(2′)	88.11(4) × 2		
–O(2″)	91.96(4) × 2		
–O(2‴)	88.04(4) × 2		
O(2)–Zr/Ta–O(2′)	180.0 × 2		
–O(2″)	90.92(1) × 2		
–O(2‴)	89.08(1) × 2		

Note. Esd's in parentheses. Bond distances in angstroms, bond angles in degrees.

TABLE 3
Cell and Atomic Parameters for $(CaZr)_{0.8}(LiTa)_{0.2}O_3$

Orthorhombic, *Pnma*, $Z = 4$
$a = 5.7076(2)$ Å, $b = 7.9670(2)$ Å, $c = 5.5492(1)$ Å

Atom	Pos.	x	y	z	B_{iso} (Å^2)	n
Ca	4(*c*)	0.0467(3)	0.25	−0.0103(5)	0.63(3)	0.80
Zr	4(*a*)	0.0	0.0	0.5	0.37(1)	0.80
Ta	4(*a*)	0.0	0.0	0.5	0.37(1)	0.20
O(1)	4(*c*)	−0.0312(3)	0.25	0.4017(3)	—	1.00
O(2)	8(*d*)	0.2978(2)	0.0515(2)	0.6987(2)	—	1.00
Li	4(*c*)	0.412(6)	0.25	0.514(8)	3.4(5)	0.20

Anisotropic temperature factors (Å^2)

	B_{11}	B_{22}	B_{33}	B_{23}	B_{13}	B_{12}
O(1)	1.12(6)	0.27(5)	0.87(5)	—	0.11(4)	—
O(2)	0.66(4)	1.01(4)	0.99(4)	0.35(3)	−0.48(3)	−0.30(3)

Note. Esd's in parentheses.

Calculation of a difference Fourier map showed the possibility of lithium atoms being located on a distorted tetrahedral site close to the calcium site. Subsequent refinements with lithium atoms located on this new site showed its site occupancy to be ~0.2, in agreement with the value expected from the chemical formula.

A close examination of the fitted profile, Fig. 3b, revealed the presence of a small number of extra reflections. These could not be accounted for by any supercell, there also being no extra reflections observed at high *d* spacings, so were assumed to be due to the presence of an impurity phase, possibly a zirconium tantalate. These regions of the profile were excluded in further structure refinements.

In the final refinements anisotropic temperature factors were successfully refined for the oxygen atoms. Refinement terminated with $R_{wp} = 2.45\%$, $R_{ex} = 1.59\%$, $\chi^2 = 2.38$ for 1788 data points and 41 variable parameters. Final refined unit cell and atomic parameters are given in Table 3 with selected bond distances and angles in Table 4.

DISCUSSION

$LiTaO_3$–$CaZrO_3$ Phase Diagram

The phase diagram for the $LiTaO_3$–$CaZrO_3$ system obtained in the present study, Fig. 1, differs in some details from that described by the previous study of Neurgaonkar *et al.* (9). This previous study was carried out at lower temperatures and appeared to concentrate more on $LiTaO_3$-rich compositions, whereas the present work, at higher temperatures, was concerned more with $CaZrO_3$-rich compositions and the new phase reported in (9).

Both phase diagrams show similar $LiTaO_3$ solid solution formation, extending to compositions containing 20 mole% $CaZrO_3$. On increasing the $CaZrO_3$ content above 20 mole%, however, differences are observed between the two sets of results. The work of Neurgaonkar *et al.* (9) reported an abrupt structural change to an "unidentified new phase" which existed for compositions containing between 21 and 70 mole% $CaZrO_3$. A two phase region then separated this new phase from $CaZrO_3$ solid

TABLE 4
Selected Bond Distances and Angles for $(CaZr)_{0.8}(LiTa)_{0.2}O_3$

Ca coordination		Li coordination	
Ca–O(1)	2.329(3)	Li–O(1)	2.60(3)
–O(1′)	2.484(3)	–O(1′)	2.33(4)
–O(2)	2.369(2) × 2	–O(2)	1.99(3) × 2
–O(2′)	2.677(2) × 2	O(1)–Li–O(1′)	84.3(13)
–O(2″)	2.811(2) × 2	–O(2)	78.9(10) × 2
–Li	0.771(33)	O(1′)–Li–O(2)	123.8(12) × 2
		O(2)–Li–O(2′)	104.9(19)
Zr/Ta coordination		O Coordination	
Zr/Ta–O(1)	2.073(1) × 2	Zr–O(1)–Zr′	147.8(1)
–O(2)	2.067(1) × 2	Zr–O(2)–Zr′	148.1(1)
–O(2′)	2.072(1) × 2		
O(1)–Zr/Ta–O(1′)	180.0		
–O(2)	91.17(6) × 2		
–O(2′)	88.83(6) × 2		
–O(2″)	91.46(6) × 2		
–O(2‴)	88.54(6) × 2		
O(2)–Zr/Ta–O(2′)	180.0 × 2		
–O(2″)	90.67(2) × 2		
–O(2‴)	89.33(2) × 2		

Note. Esd's in parentheses. Bond distances in angstroms, bond angles in degrees.

TABLE 5
Indexed Powder Data from "Unidentified New Phase" of Neurgaonkar *et al.* (9)

d_{obs}[a]	d_{calc}	$h\ k\ l$	I_{rel}
	(a) $(CaZr)_{0.21}(LiTa)_{0.79}O_3$		
3.844	3.844	0 2 0	100
2.763	2.763	2 0 0	15
2.717	2.715	1 2 1	50
2.664	2.662	0 0 2	10
2.239	2.244	2 2 0	7
2.189	2.188	0 2 2	5
1.917	1.917	2 0 2	50
1.743	1.741	3 0 1	5
1.719	1.718	1 4 1	20
1.689	1.690	1 0 3	4
1.585	1.586	3 2 1	15
	Orthorhombic, *Pnma*, a = 5.526(3) Å, b = 7.689(6) Å, c = 5.323(3) Å		
	(b) $(CaZr)_{0.70}(LiTa)_{0.30}O_3$		
3.952	3.948	0 2 0	75
2.827	2.823	2 0 0	25
2.790	2.786	1 2 1	100
2.741	2.738	0 0 2	20
2.296	2.296	2 2 0	5
2.248	2.250	0 2 2	8
1.969	1.974	0 4 0	45
	1.965	2 0 2	
1.778	1.778	0 1 3	10
1.761	1.764	1 4 1	25
	1.759	2 2 2	
1.734	1.737	1 0 3	5
	1.736	3 1 1	
1.622	1.622	3 2 1	20
	Orthorhombic, *Pnma*, a = 5.645(4) Å, b = 7.896(12) Å, c = 5.475(3) Å		

[a] d_{obs} calculated from 2θ data given in Table 2, Ref. (9).

solutions, which were formed between 94 and 100 mole% $CaZrO_3$.

In the present phase diagram study a two-phase region is observed between 20 and 27 mole% $CaZrO_3$, which separates $LiTaO_3$ and $CaZrO_3$ solid solutions. Moreover, the unidentified phase of (9) has been shown to be part of an extended region of $CaZrO_3$ solid solutions extending from 27 to 100 mole% $CaZrO_3$ and having an immiscibility gap present for compositions between 88 and 95% $CaZrO_3$. It is clear that our results are broadly consistent with those of Neurgaonkar *et al.* (9) and that their unidentified new phase corresponds to our extended $CaZrO_3$ solid solution phase field. It was also found here that the (unindexed) powder X-ray diffraction data reported in (9), which corresponded to the composition limits of their new phase, could be indexed on a similar orthorhombic unit cell to that of $CaZrO_3$ (17), Table 5. Furthermore, it is highly likely that the two phase region reported in (9) between 70 and 94 mole% $CaZrO_3$ corresponds to the immiscibility gap described here.

The results from the structure refinement of the $(CaZr)_{0.8}(LiTa)_{0.2}O_3$ composition, showing that this phase has a perovskite-like structure similar to that of orthorhombic $CaZrO_3$, confirm those from the present phase diagram study.

Structure Refinements

$(CaZr)_{0.97}(LiTa)_{0.03}O_3$. This material, Fig. 4, is an orthorhombic perovskite solid solution. Ta substitutes for Zr on the octahedral B sites and the BO_6 octahedra are very regular, with all six M–O bond distances almost identical and O–M–O bond angles very close to 90 and 180°, Table 2. Since Ta and Zr have similar bond distances to oxygen (2.04 and 2.12 Å, respectively) and since both are highly charged this substitution is not unfavorable (although Zr and Ta chemistries are usually considered to be different). As another example, Ta and Zr are disordered over the same sets of octahedral and distorted octahedral sites in $LaZrTa_3O_{11}$ (18).

Although it has a similar typical octahedral M–O bond distance (2.14 Å) to Zr and Ta, lithium possibly would not be stable on the B site due to its single positive charge. Nevertheless, lithium has been shown to occupy half the octahedral B sites in the ordered perovskite La_2LiSbO_6, with the rest of the B sites occupied by antimony (19).

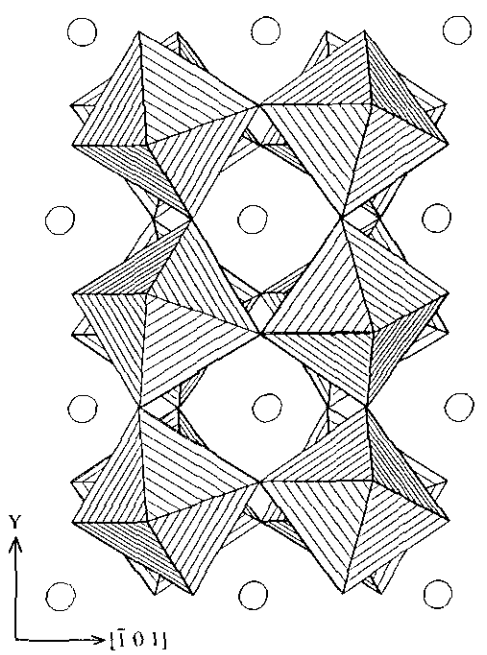

FIG. 4. Polyhedral representation of the crystal structure of $(CaZr)_{0.97}(LiTa)_{0.03}O_3$ projected along [1 1 0]. Octahedra represent (Zr, Ta)O_6; circles represent Ca/Li.

The large *A* site is fully occupied, containing both calcium and lithium atoms. The calcium coordination, which is lowered from 12- to 8-fold coordination by the orthorhombic distortion, is essentially that of a distorted square antiprism and a range of Ca–O bond distances is observed, Table 2. This spread of Ca–O bond distances is also seen in stoichiometric $CaZrO_3$ (15). Lithium, which also partially occupies this site, is assumed to be coordinated by the shortest four *A*–O distances which form a distorted tetrahedral environment. Although this is rather a large site, which may be considered too large for lithium to occupy, the refined site occupancies for lithium and calcium on this site agreed well with those expected from the chemical formula.

Because of its smaller size, the thermal vibration about the mean position is likely to be greater for lithium than for calcium, although their structural parameters (in particular their isotropic temperature factors) had to be constrained to be equal in the least squares refinement. Certainly, the contrast provided by the difference in neutron scattering lengths should facilitate the detection of any site separation, if present. Nevertheless, the low doping level would strongly constrain the lithium to occupy the calcium sites.

$(CaZr)_{0.8}(LiTa)_{0.2}O_3$. The structure refinement results show that $(CaZr)_{0.8}(LiTa)_{0.2}O_3$ also has an orthorhombic perovskite-like structure, very similar to that of $(CaZr)_{0.97}(LiTa)_{0.03}O_3$ with Zr and Ta disordered over the octahedral B sites, Fig. 5. The BO_6 octahedra again are almost undistorted, Table 4.

The large cavity formed by the BO_6 octahedra still accommodates both the Ca and Li atoms. However, since typical Li–O bond distances are ~0.45 Å shorter than typical Ca–O bond distances, at this composition two sets of sites are occupied. Calcium is present with partial occupancy on the same sites as in $CaZrO_3$ and $(CaZr)_{0.97}(LiTa)_{0.03}O_3$ and is coordinated to 8 oxygens in a distorted square antiprism arrangement. The lithium site is situated ~0.77 Å from the center of the Ca site, displaced, approximately along the $[\bar{1}00]$ direction towards a neighbouring O(1) atom. This produces a grossly distorted tetrahedral environment for lithium, having two (symmetry equivalent) Li–O bond distances with typical values, and two somewhat longer Li–O bonds, Table 4. The distortion in bond angles means that lithium has an almost trigonal pyramidal coordination.

In the $CaZrO_3$ solid solutions, a definite trend is observed in the Zr–O–Zr bond angles, Table 6. In stoichiometric $CaZrO_3$, the Zr–O(1)–Zr angle is 146.5° and the Zr–O(2)–Zr angle 145.8°. In the solid solutions both angles increase slightly, the larger increase, of ~2.3°, occurring in the Zr–O(1)–Zr angle. As these angles are the tilt angles between corner sharing BO_6 octahedra (equal to 180° in the ideal cubic perovskite structure) it follows that the twisting of the octahedra decreases on increasing the Li TaO_3 content. This is manifest also in the orthorhombic distortion of $CaZrO_3$ which decreases slightly with increasing solid solution formation.

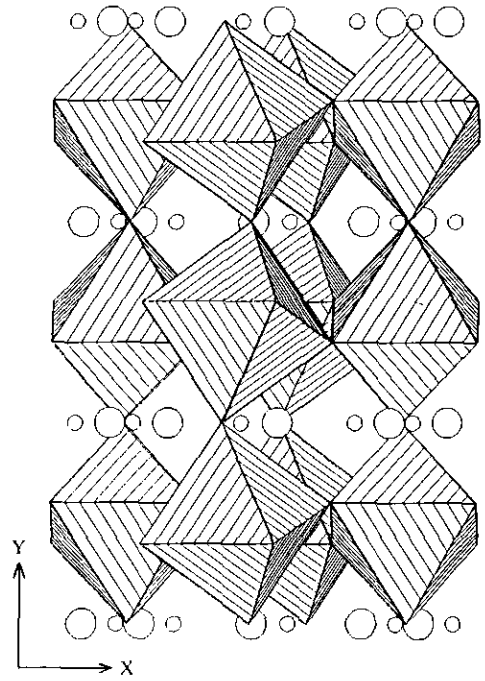

FIG. 5. Polyhedral representation of the crystal structure of $(CaZr)_{0.8}(LiTa)_{0.2}O_3$ projected along *z* and rotated ~12° round *y*. Octahedra represent $(Zr,Ta)O_6$; large circles represent Ca; small circles represent Li.

This decrease in the distortion would increase the size of the cavity containing the Ca and Li atoms, an unexpected situation considering the substitution of calcium by smaller lithium atoms. Instead, it is compensated by a decrease in unit cell parameters which reduces the size of the cavity and which is associated with a decrease of the average Zr/Ta–O bond distance. This is reasonable since Ta–O bond distances are typically ~0.08 Å less than Zr–O distances (20).

TABLE 6
Variation in Zr–O–Zr Bond Angles in $CaZrO_3$ Solid Solutions

	Zr–O(1)–Zr	Zr–O(2)–Zr
$CaZrO_3$[a]	145.8°	146.5°
$(CaZr)_{0.97}(LiTa)_{0.03}O_3$	146.00°	147.19°
$(CaZr)_{0.8}(LiTa)_{0.2}O_3$	147.85°	148.09°

Note. Angles taken from Tables 2 and 4.
[a] Bond angles calculated from data given in Ref. (15).

Solid Solution Immiscibility

The exact cause of the $CaZrO_3$ solid solution immiscibility is not known, but is almost certainly associated with the substitution of Ca and Zr by Li and Ta. Probably, the location of lithium on a separate site in $(CaZr)_{0.8}(LiTa)_{0.2}O_3$ is significant. Separate sites were not observed in the 97 : 3 mole% composition, with both Li and Ca atoms occupying the same position. The *A* site is rather large so lithium is expected to be unstable on it. However, perhaps a few mole% lithium can be located on the Ca site before it becomes unstable. It is then forced to occupy its own separate site which gives rise to a small distortion of the octahedral framework.

It may be that a certain minimum lithium content is required to achieve this. Thus, at lower lithium contents, e.g., 10% $LiTaO_3$, there may be too much lithium to occupy the *A* site but insufficient to cause a change to occupancy of the distorted tetrahedral site. Consequently, an immiscibility region exists.

The plots of unit cell parameters versus composition, Fig. 2, appear to show a different slope on either side of the compositions where solid solution immiscibility occurs. This feature is more marked with the *b* and *c* cell edges, and may actually be due simply to the limited number of data points for compositions containing >95 mole% $CaZrO_3$. However, departures from Vegard's law such as this, in which the lattice parameters of intermediate compositions are higher than those expected from a straight line plot passing through the end-member data points, have been postulated previously as being indicative of the formation of immiscibility domes (21). Our results are consistent therefore with this suggestion.

CONCLUSIONS

The unidentified new phase reported by Neurgaonkar *et al.* is an orthorhombic, perovskite-like, $CaZrO_3$ solid solution with the replacement mechanism

$$Ca + Zr = Li + Ta.$$

Ta and Zr appear to disorder over the octahedral *B* sites of the perovskite structure. Li is generally too small to occupy the 8-coordinate *A* sites and, for most of the solid solutions, occupies an off-center, distorted tetrahedral site within the same cavity as the *A* sites. At low Li contents, ~5–12% $LiTaO_3$, an immiscibility region exists in the solid solutions which is probably caused by subtle structural changes associated with relocation of Li into the tetrahedral sites; a certain minimum level of occupancy may be necessary in order to stabilize the structure.

ACKNOWLEDGMENTS

We would like to thank the U.K. Science and Engineering Research Council for financial support and the allocation of neutron beam time and J. G. Fletcher and K. M. Cruickshank for assistance in measuring unit cell parameters. Crystal structures were drawn using the STRUPLO plotting program (22).

REFERENCES

1. B. T. Matthias and J. P. Remeika, *Phys. Rev.* **76,** 1886 (1949).
2. K. Nassau, H. J. Levinstein, and G. M. Loiacono, *Appl. Phys. Lett.* **6,** 228 (1965).
3. K. Nassau, H. J. Levinstein, and G. M. Loiacono, *J. Phys. Chem. Solids* **27,** 983, 989 (1966).
4. B. Guenais, M. Baudet, M. Minier, and M. Le Cun, *Mater. Res. Bull.* **16,** 643 (1981).
5. R. V. Schmidt and I. P. Kaminow, *Appl. Phys. Lett.* **25,** 458 (1974).
6. J. Noda, N. Uchida, S. Saito, and M. Minakata, *Appl. Phys. Lett.* **27,** 19 (1975).
7. C. E. Rice, *J. Solid State Chem.* **64,** 188 (1986).
8. M. E. Villafuerte-Castrejón and A. R. West, personal communication (1989).
9. R. R. Neurgaonkar, T. C. Lim, and E. J. Staples, *Mater. Res. Bull.* **13,** 635 (1978).
10. M. A. Hepworth and K. H. Jack, *Acta Crystallogr.* **10,** 345 (1957).
11. M. E. Villafuerte-Castarejón, C. Kuhliger, R. Ovando, R. I. Smith, and A. R. West, *J. Mater. Chem.* **1,** 747 (1991).
12. H. M. Rietveld, *J. Appl. Crystallogr.* **2,** 65 (1969).
13. (*a*) W. I. F. David, D. E. Akporiaye, R. M. Ibberson, and C. C. Wilson, Report RAL-88-103, Rutherford Appleton Laboratory, 1988; (*b*) P. J. Brown, and J. C. Matthewman, Report RAL-87-010, Rutherford Appleton Laboratory, 1987.
14. L. Koester and H. Rauch, Report 2517/RB, International Atomic Energy Agency, Vienna (1981).
15. H. J. A. Koopmans, G. M. H. van de Velde, and P. J. Gellings, *Acta Crystallogr. Sect. C* **39,** 1323 (1983).
16. (*a*) International Tables for Crystallography (T. Hahn, Ed.), Vol. A. Kluwer Academic, Dordrecht, 1983; (*b*) International Tables For X-Ray Crystallography (N. F. M. Henry and K. Lonsdale, Eds.), Vol. I. Kynoch Press, Birmingham (1969).
17. JCPDS cards 35-645 and 35-790.
18. J. Grins, M. Nygren, C. Zheng, and A. R. West, *Mater. Res. Bull.* **27,** 141 (1992).
19. (*a*) M.L. López, M. L. Veiga, A. Jerez, and C. Pico, *Mater. Res. Bull.* **25,** 1271 (1990). (*b*) M. L. López, M. L. Veiga, J. Rodríguez-Carvajal, F. Fernández, A. Jerez, and C. Pico, *Mater. Res. Bull.* **27,** 647 (1992).
20. (*a*) R. D. Shannon and C. T. Prewitt, *Acta Crystallogr. Sect. B* **25,** 925(1969); (*b*) R. D. Shannon and C. T. Prewitt, *Acta Crystallogr. Sect. B* **26,** 1046 (1970).
21. M. Castellaños and A. R. West, *J. Chem. Soc. Faraday Trans. 1* **76,** 2159 (1980).
22. R. X. Fischer, *J. Appl. Crystallogr.* **18,** 258 (1985).